



## Pyrometallurgical strategies for recycling SmCo permanent magnets: A comprehensive review

Mehrdad Gharavi<sup>a,1</sup>, Sara Karimi Moghadam<sup>b,1</sup>, Ali Asimi Neisiani<sup>c,d,\*</sup> , Carina Ulsten<sup>c,d</sup>, Saeed Chehreh Chelgani<sup>e,f,\*\*</sup> 

<sup>a</sup> Department of Materials Science and Engineering, Sharif University of Technology, Tehran, 14584-33111, Iran

<sup>b</sup> School of Metallurgy and Materials Engineering, Iran University of Science and Technology (IUST), Tehran, 16846-13114, Iran

<sup>c</sup> Department of Mining and Petroleum Engineering, Polytechnic School, University of São Paulo (USP), Sao Paulo, SP, 05508-900, Brazil

<sup>d</sup> Technological Characterization Laboratory, Department of Mining and Petroleum Engineering, Polytechnic School of the University of Sao Paulo (USP), Sao Paulo, SP, 05508-900, Brazil

<sup>e</sup> Minerals and Metallurgical Engineering, Department of Civil, Environmental and Natural Resources Engineering, Swedish School of Mines, Luleå University of Technology, Luleå, 97187, Sweden

<sup>f</sup> Wallenberg Initiative Materials Science for Sustainability, Department of Civil, Environmental and Natural Resources Engineering, Swedish School of Mines, Luleå University of Technology, Luleå, 97187, Sweden

### ARTICLE INFO

#### Keywords:

REE  
Recycling  
Permanent Sm-Co magnets  
Pyrometallurgy  
Sustainability

### ABSTRACT

Samarium-cobalt (Sm-Co) permanent magnets are widely used in high-temperature, high-performance applications, but their recycling is difficult due to their thermal stability and complex alloy chemistry. However, the strategic and economic importance of Sm and Co makes the development of efficient recycling routes increasingly critical. This review focuses on pyrometallurgical approaches for recovering Sm and Co from end-of-life magnets and industrial scrap. Thermal pretreatment, such as demagnetization near or above the Curie temperature (~720–820 °C), not only removes magnetic properties but also promotes surface oxidation, producing more reactive oxide phases that facilitate subsequent processing. Among pure thermal routes, vacuum distillation exploits differences in vapor pressure to selectively evaporate Sm under reduced pressure. Recovery efficiency and final purity depend strongly on precise temperature control and the choice of condenser material. Molten salt extraction in LiCl-KCl eutectics uses oxygen sparging to convert SmCl<sub>3</sub> into SmOCl while leaving Co in the melt, enabling phase separation. The glass slag technique with molten B<sub>2</sub>O<sub>3</sub> transfers Sm into the slag as Sm<sub>2</sub>O<sub>3</sub>/SmBO<sub>3</sub> and yields Co or Fe-rich alloys with very low Sm content. Hybrid pyro-hydrometallurgical methods, notably nitric acid baking followed by controlled thermal decomposition, exploit the differing thermal stabilities of Sm, Co, and Fe nitrates to selectively dissolve Sm while converting base metals to insoluble oxides. Sulfation and selective oxidation are additional thermal steps that can improve phase separation prior to aqueous recovery. Moreover, solid-state chlorination showed a higher reactivity of Sm toward HCl (with Co being less reactive) under optimal conditions. Drawing together the latest findings and emerging trends, this review highlights the key technical challenges, critical knowledge gaps, and promising opportunities. This work examined the feasibility of all reported chemical reactions and assessed them using Gibbs energy. It also sets out focused research priorities to accelerate the development and wider adoption of pyrometallurgical strategies for Sm-Co magnet recycling. Particular emphasis is placed on energy-efficient demagnetization and volatilization, impurity-tolerant molten salt and slag chemistries, durable condenser materials, emissions control, and practical integration with hydrometallurgical steps.

\* Corresponding author. Department of Mining and Petroleum Engineering, Polytechnic School, University of São Paulo (USP), Sao Paulo, SP, 05508-900, Brazil.

\*\* Corresponding author. Minerals and Metallurgical Engineering, Department of Civil, Environmental and Natural Resources Engineering, Swedish School of Mines, Luleå University of Technology, Luleå, 97187, Sweden.

E-mail addresses: [ali.asimi@usp.br](mailto:ali.asimi@usp.br) (A.A. Neisiani), [saeed.chelgani@ltu.se](mailto:saeed.chelgani@ltu.se) (S.C. Chelgani).

<sup>1</sup> The first two authors contributed equally to this project.

<https://doi.org/10.1016/j.mtsust.2026.101392>

Received 17 March 2026; Received in revised form 12 May 2026; Accepted 18 May 2026

Available online 18 May 2026

2589-2347/© 2026 The Author(s). Published by Elsevier Ltd. This is an open access article under the CC BY license (<http://creativecommons.org/licenses/by/4.0/>).

### 1. Introduction

Samarium (Sm) and Cobalt (Co) are crucial elements classified globally as critical raw materials (CRMs) due to their geopolitical supply risk, economic significance, and irreplaceable roles in advanced technological systems [1–3]. Samarium-Cobalt (Sm-Co) permanent magnets “PMs”, typically formulated as  $\text{SmCo}_5$  or  $\text{Sm}_2\text{Co}_{17}$  alloys, are fundamental to modern industrial infrastructure and a low-carbon economy [4–6]. Sm-Co PMs offer distinct advantages over neodymium-iron-boron (Nd-Fe-B) magnets, including superior corrosion resistance, higher coercivity, and exceptional thermal stability. They typically operate at temperatures in the high 300 °C range, and some reports indicated that they can retain their magnetic strength even under more severe thermal conditions, up to 550 °C [3,7–10]. Consequently, Sm-Co magnets are crucial for specialized, high-performance sectors such as aerospace, national defense, military equipment, and high-temperature automotive applications (Fig. 1) [11,12]. This sustained, and specialized demand underscores the critical status of their constituent rare earth elements (REEs) and Co, both of which are projected to face supply-side pressures as global requirements increase by 3-7 times between 2020 and 2040 [13,14].

However, the manufacturing of Sm-Co magnets is highly resource-intensive, with approximately 15-30% of raw materials generated as waste streams, including swarf and scraps [15–17]. End-of-life Sm-Co magnets and manufacturing rejects constitute a valuable secondary resource rich in Sm (20-40 %) and Co (45-60 %), presenting a significant opportunity for resource valorization. The composition of this secondary source (Fig. 2) typically includes co-existing metals such as iron (Fe), copper (Cu), and Zirconium (Zr) [9,12,18,19]. Therefore, recycling these critical components not only improves supply vulnerability but also minimizes the substantial environmental burden associated with conventional mining and mineral processing [15,20,21]. Developing efficient and sustainable recovery methodologies is critical for realizing a comprehensive circular economy for these strategic materials and enabling their reuse across various applications and industries.

Current methodologies for recovering value-added products from spent magnets are predominantly classified as hydrometallurgical or pyrometallurgical [5,22]. Hydrometallurgy, typically using acid leaching and downstream purification (e.g., solvent extraction or deep eutectic solvents), offers excellent product purity and operates at moderate temperatures [5,23,24]. Nevertheless, this route is frequently

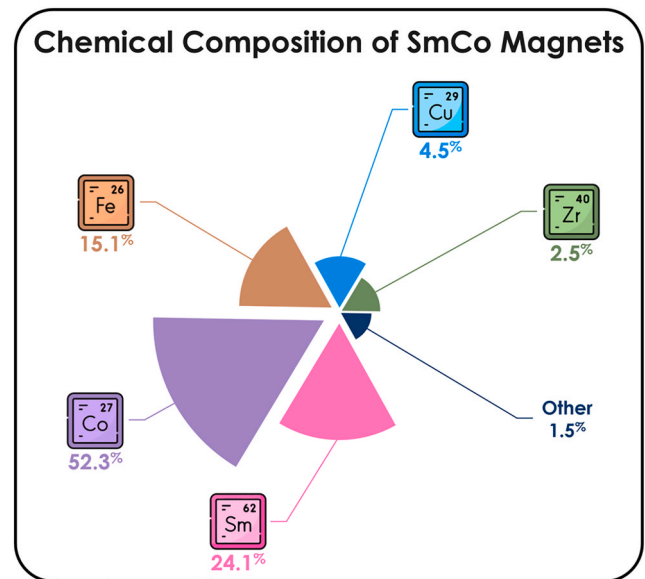


Fig. 2. Average elemental composition (%) of Sm-Co magnets.

characterized by substantial water and reagent consumption, complex wastewater discharge, and high overall operational complexity, posing significant environmental drawbacks [25–27]. Conversely, pyrometallurgical strategies rely on elevated thermal conditions to promote phase separation or drive selective volatilization [28–31]. Pyrometallurgical routes offer inherent benefits for recycling PMs, including high throughput and tolerance of impure feedstock. Additionally, because it requires no complex pretreatment and is insensitive to feed composition, it is a relatively rapid process [32,33]. Moreover, thermal techniques play a crucial role beyond pure pyrometallurgy, offering support to hydrometallurgical processes at various stages (Fig. 3). This includes thermal demagnetization (before hydrometallurgy) to improve leaching kinetics, forming hybrid pyro-hydro routes, and subsequent thermal steps like calcination for producing high-purity metal oxides after hydrometallurgical separation [18,34,35]. However, they require high energy inputs and demand stringent control over harmful gaseous emissions and solid waste (slag) generation [28,36]. The technical

### Various Applications of SmCo Permanent Magnets

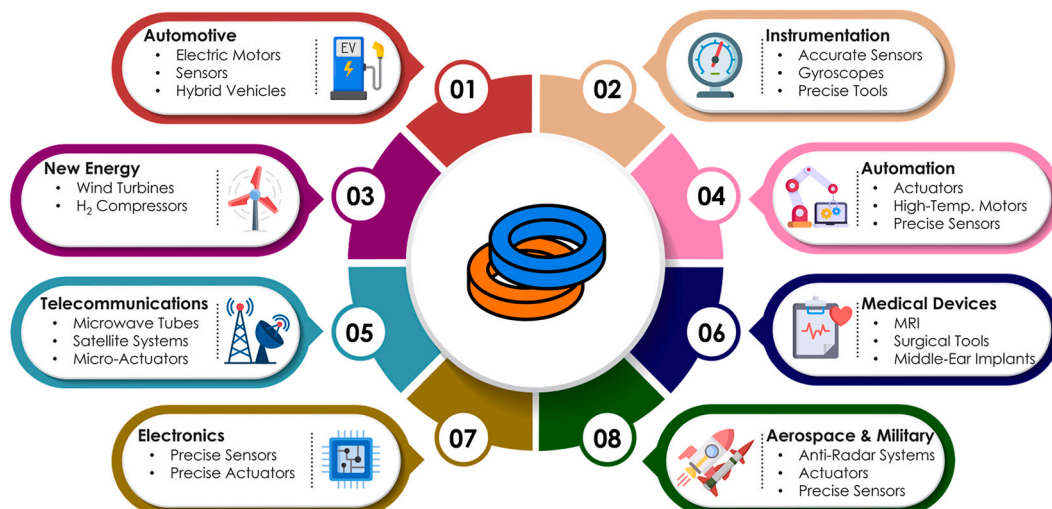


Fig. 1. Various applications of the Sm-Co magnets.

## Thermal-Based Processes in SmCo Magnet Recovery

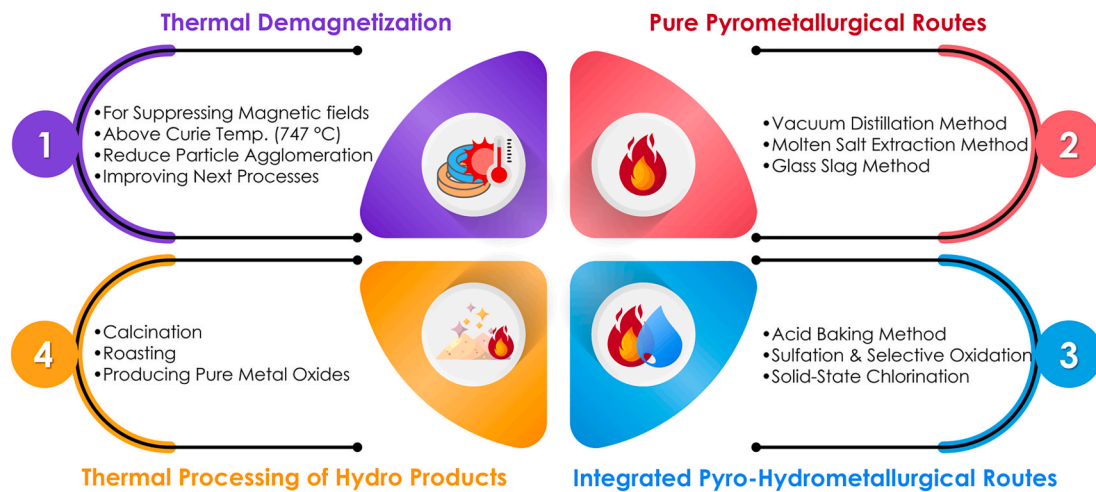


Fig. 3. Thermal processes for recycling Sm-Co magnets.

challenges and environmental constraints associated with both pure pyro- and integrated hydro-pyro-metallurgical methods necessitate focused research into innovative, cleaner thermal processes for Sm-Co magnet recycling [8,28].

Despite the significance and unique status of Sm-Co magnets, there is still no comprehensive assessment of the published research on the pyrometallurgical processes used in their recovery. This work will fill this gap by providing an in-depth analysis and comparison of existing studies on thermal-based recycling technologies, critically evaluating their underlying mechanisms, efficiencies, and limitations. It provides a comprehensive evaluation across several distinct phases of thermal application in recycling flowsheets. The analysis begins with thermal demagnetization and essential preprocessing steps, which often involve roasting to convert metallic phases into reactive oxides or to prepare feed for subsequent leaching. It then critically examines various pure pyrometallurgical routes (including vacuum distillation, molten salt, glass slag techniques, and selective oxidation), which aim for selective extraction and concentration of Sm and Co. Subsequently, details of integrated pyro-hydrometallurgical routes (e.g., acid baking and solid-state chlorination) designed to leverage the selectivity of pyrometallurgy while minimizing the drawbacks of absolute hydrometallurgy are analyzed. Finally, this study is willing to address the crucial thermal processing of hydro products, specifically the calcination of intermediate precipitates (e.g., oxalates) to yield high-purity final products, such as  $\text{Sm}_2\text{O}_3$  and  $\text{Co}_3\text{O}_4$ . Throughout, this work highlights inconsistencies in the literature, elucidates dominant reaction pathways, and identifies critical knowledge gaps and future research needs.

### 2. Thermal demagnetization

The demagnetization process is primarily intended to eliminate the alloys' intrinsic magnetic properties. This prevents the adhesion of magnetic powders to metallic equipment during handling and processing [5,12,23]. Additionally, demagnetization helps break down powder agglomerates and enhances the leachability of the material when hydrometallurgy is used as the next processing stage [11,12]. Sm-Co magnets possess exceptionally high Curie temperatures ( $T_C$ ). The  $T_C$  of this permanent magnet can exceed  $\sim 720$  °C for  $\text{SmCo}_5$  and  $\sim 820$  °C for  $\text{Sm}_2\text{Co}_{17}$ , which significantly surpasses the 310 °C threshold observed in Nd-Fe-B magnets [37–39]. Demagnetization typically involves heating the magnetic material to temperatures approaching or exceeding its  $T_C$ ,

the threshold at which the ferromagnetic structure transforms into a paramagnetic state. This stage results in the random orientation of the magnetic dipoles and macroscopic demagnetization [5,11].  $T_C$  of materials varies with chemical composition, explaining the difference between the  $T_C$  of Nd-Fe-B and Sm-Co magnets, as well as between various types of Sm-Co magnets (Fig. 4) [8,11]. This variation explains the greater thermal stability and resistance of Sm-Co magnets to demagnetization, a property that underpins their extensive use in high-temperature applications [8,28,41].

During demagnetization, when tempering Sm-Co magnets between 450 °C and 800 °C, a distinct agglomerate decomposition occurs at sub-

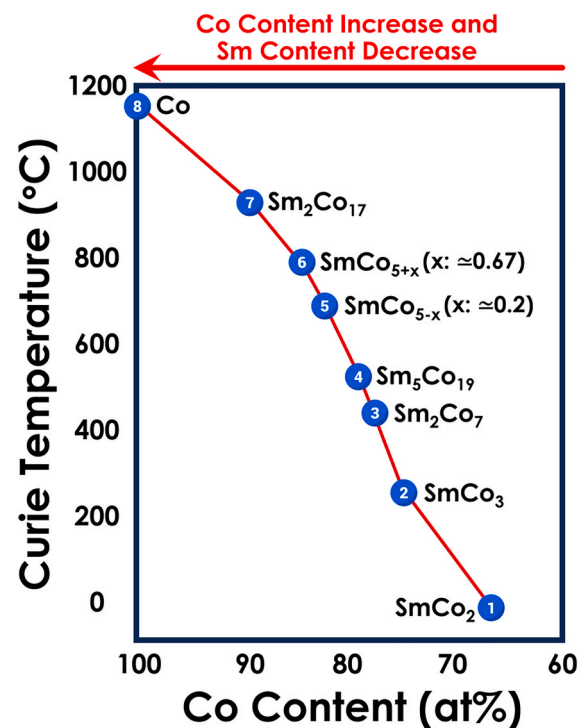


Fig. 4. Sm-Co system phase diagram as a function of temperature and Co content (Based on [40]).

Curie temperatures. At 450 °C, many magnet particle agglomerates were reported to be partially separated. As the temperature increased to 600 °C, the proportion of particles smaller than 100 μm rose from 14.5% to 81.7%. However, heating above this range (600-800 °C) produced no further decrease in particle size. It indicated that physical disintegration predominated below the  $T_C$ , whereas complete demagnetization occurred only beyond it.  $T_C$  for SmCo<sub>5</sub> alloys marked the transition to a paramagnetic state in which Weiss domains vanished, and dipole alignment collapsed completely [11]. Upon cooling, new magnetic domains partially reformed, particularly in particles smaller than 1.5 μm (approximately the size of a single Weiss domain), resulting in partial re-magnetization. Correspondingly, magnetic flux density decreased from 200 to 240 μT in untreated samples to 140-180 μT in thermally treated powders. This confirmed a progressive loss of magnetization due to domain misalignment at sub-Curie temperatures and an irreversible collapse at super-Curie conditions [11].

Beyond magnetic effects, demagnetization drives critical structural and chemical transformations that facilitate downstream hydrometallurgical recovery. Thermal oxidation during heating converts SmCo<sub>5</sub> alloys into stable oxides, such as SmCoO<sub>3</sub> and Co<sub>3</sub>O<sub>4</sub>, which exhibit higher chemical reactivity and increased surface porosity relative to the metallic precursor [11,12,41]. Sinha et al. (2017) reported that complete conversion occurred after roasting at approximately 850 °C for 6 h in an air atmosphere, as confirmed by X-ray diffraction (XRD), scanning electron microscopy (SEM), and energy-dispersive spectroscopy (EDS) analyses [12]. The resulting oxide phase enhanced leachability by enlarging surface area and disrupting the dense metallic structure. Thermogravimetric analysis indicated a weight gain of approximately 27% at 850 °C, consistent with oxygen uptake during oxidation and phase transformation. Subsequent chemical analyses revealed final compositions of 30.4% Sm and 42.6% Co in the oxidized product [12]. In contrast to Nd-Fe-B magnets, Sm-Co powders exhibit limited reactivity with oxygen, minimizing the risk of spontaneous combustion and rendering demagnetization operations considerably safer [5,41].

However, the inherent magnetocrystalline anisotropy of Sm-Co alloys poses a significant challenge [8,12]. High magnetocrystalline energy barriers render Sm-Co magnets highly resistant to both magnetic and thermal demagnetization, thereby necessitating prolonged high-temperature treatment [8,16,42]. To achieve full demagnetization and oxide formation, temperatures of 800-900 °C and longer residence times are often required, especially in pyrometallurgical or gas-phase extraction routes [5,8,12]. It is also worth noting that demagnetizing Sm-Co magnets requires more energy than demagnetizing Nd-Fe-B magnets because Sm-Co magnets have a significantly higher Curie temperature. However, Sm-Co's resistance to heat allows it to retain magnetism even after a complete loss of magnetism if the process is handled correctly. Although the process is energy-intensive compared with demagnetizing Nd-Fe-B magnets, the thermal robustness of Sm-Co alloys ensures complete removal of magnetic effects under appropriately controlled conditions [3,8,12,16,18,43]. Despite the importance of thermal demagnetization, research on its thermal behavior and microstructural evolution during pretreatment is limited. Additionally, the fundamental mechanisms governing demagnetization and oxidation kinetics in Sm-Co magnets remain insufficiently understood, necessitating further investigation to optimize recycling efficiency and energy use.

### 3. Pyrometallurgical routes

#### 3.1. Vacuum distillation

The vacuum distillation method, recognized as a promising green pyrometallurgical route, enables the selective extraction of Sm from Sm-Co magnet waste by exploiting thermodynamic differences among the constituent metals. The significantly lower melting and boiling points of Sm (1072 and 1791 °C, respectively) than those of the other associated

elements (Co, Fe, Cu, and Zr (Table 1) facilitate its preferential evaporation under reduced pressure. Sm-Co magnet scrap starts to melt at 1311 °C and begins to deform between 1321 and 1452 °C, during which Sm evaporates readily due to its relatively high vapor pressure. The saturated vapor pressure of Sm increases sharply with temperature, enabling its selective transition into the vapor phase before other alloying metals [44].

Bai et al. (2024) designed a high-temperature vacuum distillation furnace equipped with a vertical two-temperature-zone extraction system. The heating system comprised independently controlled upper and lower zones, permitting efficient evaporation and condensation of metal vapors (Fig. 5). A double condensation collector was integrated to ensure high-purity collection of Sm, with the metal vapor of higher vapor pressure enriched in the upper condenser, while impurity elements with lower vapor pressures were effectively separated. Experimental investigations were carried out in the temperature range of 1300-1500 °C under a vacuum of approximately  $8 \times 10^{-3}$  Pa to evaluate the influence of temperature on the evaporation-condensation behavior of Sm from Sm-Co magnet scrap [44].

The evaporation rates of various metals, including Sm, Co, Fe, Cu, and Zr, were examined between 1200 and 1700 °C. Results confirmed that the evaporation rates of all metals increased with temperature at constant pressure. However, at equivalent temperatures and times, Sm exhibited a substantially higher evaporation rate than the other elements. During vacuum distillation, when phase transformation occurs, the system pressure remains below the materials' saturation vapor pressure. Therefore, metals with higher vapor pressure, especially Sm, tend to evaporate preferentially. The condensation rate of Sm between 1400 and 1600 °C was also measured, showing that its effective condensation temperature range lies between 600 and 900 °C. To achieve efficient condensation while minimizing contamination, the condensation zone was thermally isolated from the heating zone [44].

The interaction between condensers and REE vapors played a crucial role in determining the recovery efficiency and the purity of Sm, owing to REEs' high reactivity and physicochemical activity. The influence of graphite, tantalum (Ta), and molybdenum (Mo) condensers on Sm enrichment showed that when graphite served as the condenser, the major condensate constituents were Sm and C, suggesting the potential for REE carbide formation at elevated temperatures. The coexistence of nonmetallic impurities such as carbon, nitrogen, and oxygen in the condensates indicated the formation of intermediate compounds through reactions with the condenser surface. The Ta condenser collected only a small amount of Sm, while a substantial portion condensed on the sidewalls of the crucible. In contrast, the Mo condenser demonstrated superior performance, with a Sm enrichment rate exceeding 95%. According to the Sm-Ta and Sm-Mo phase diagrams, no solid solution or intermetallic compounds formed between Sm and these refractory metals. However, the solubility of Sm in Ta is slightly higher than in Mo, confirming Mo as the optimal condenser material for Sm recovery [44]. It was concluded that precise temperature control is vital. While higher temperatures promote complete Sm evaporation, they also enhance volatilization of impurity metals, degrading product purity. Conversely, insufficient temperature hinders Sm volatilization, thereby reducing REE recovery. Thus, an optimal balance must be maintained, keeping the temperature sufficiently high to sustain both recovery efficiency and product purity [44]. These observations also demonstrate the important role of impurity elements in governing separation selectivity during vacuum distillation. In

**Table 1**

Melting and boiling temperatures of the main elements composing Sm-Co magnets (Based on [44]).

Element	Sm	Co	Fe	Cu	Zr
Melting point (°C)	1072	1495	1538	1085	1852
Boiling point (°C)	1791	2870	2800	2562	4377

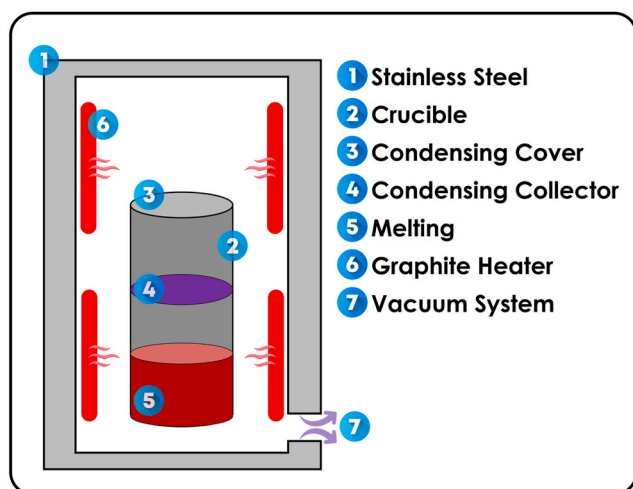


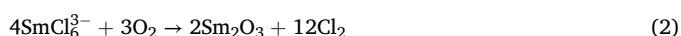
Fig. 5. Schematic illustration of high-temperature vacuum distillation and condensation setup used for Sm extraction from Sm-Co magnet scrap (Based on [44]).

particular, Cu is the most important impurity because its relatively high vapor pressure promotes coevaporation at elevated temperatures, whereas Fe and Zr largely remain in the residual phase due to their low volatility. Consequently, impurity-dependent volatilization behavior defines the practical temperature window required to simultaneously maximize Sm recovery and maintain product purity [44].

Despite the progress achieved, further studies are required to systematically examine the interactions between different condenser materials and Sm vapor. In particular, the potential of other high-melting-point metals or coated surfaces to enhance selectivity has been largely overlooked. Additionally, the long-term stability of the condenser has not yet been evaluated. The current research also does not address the influence of impurities such as oxygen, nitrogen, or carbon within the system, nor does it assess how the alloy's microstructure or oxidation state affects the kinetics of Sm evaporation. Given the critical importance of economic feasibility and energy efficiency, no comparative analysis with hydrometallurgical routes or alternative recovery methods has been conducted.

### 3.2. Molten salt extraction (alkali chloride melts)

The recovery and selective extraction of REEs as chlorides through oxidation in molten alkali chloride media have been examined in some investigations. In this technique, a binary eutectic system of LiCl-KCl (3LiCl-2KCl) has shown promise for separating Sm and Co chlorides via oxygen sparging. The experiments were conducted over the temperature range 400-700 °C, using Sm(III) chloride ( $\text{SmCl}_3$ ) and Co(II) chloride ( $\text{CoCl}_2$ ) dissolved in the melt. The eutectic mixture was prepared by melting appropriate amounts of Li and K chlorides, and Sm and Co chlorides were introduced using hydrogen chloride gas. The primary mechanism driving the separation of Sm and Co was found to be the difference in their oxygen affinities, which governs their distinct oxidation behaviors within the molten chloride environment [16]. Thermodynamic analyses and experimental results consistently indicated that Sm chloride reacted readily with oxygen to form Sm oxychloride ( $\text{SmOCl}$ ), whereas Co chloride remained largely unreactive under identical conditions. The reactions describing this behavior could be expressed as (Equ. 1-4):



The Gibbs free energy change for  $\text{SmOCl}$  formation at 700 °C was determined to be  $-67.8$  kJ/mol, confirming that  $\text{SmOCl}$  formation is thermodynamically feasible, whereas the similar Co oxidation route is unlikely. Consequently, during oxygen sparging in the LiCl-KCl system at temperatures up to 700 °C,  $\text{SmOCl}$  remained the sole solid product, regardless of oxygen concentration, whereas Co remained molten. It was concluded that both the temperature and oxygen content control the extent of  $\text{SmOCl}$  formation. At 600 °C, the initial Sm concentration had a limited effect on the reaction rate, whereas at 700 °C, a pronounced concentration dependence was observed, with higher Sm concentrations accelerating oxychloride formation. Kinetic analysis revealed a first-order dependence on  $\text{SmCl}_3$ , with an activation energy of 57.9 kJ/mol [16].

The LiCl-KCl eutectic melt also functions as a reusable reaction medium, improving the environmental sustainability of the pyrochemical recovery process. The selectivity of this route stems from the preferential formation of sparingly soluble  $\text{SmOCl}$ , which readily separates from the melt, while cobalt remains dissolved as  $\text{CoCl}_2$ . Experimental studies showed that  $\text{SmOCl}$  precipitates can be separated from the liquid phase by controlled settling, followed by decantation or sampling. To maintain salt regeneration and process continuity, dissolved cobalt can subsequently be recovered electrochemically, thereby removing accumulated transition metals from the molten medium before reuse in successive cycles. Although the process still requires high-temperature operation and relatively costly alkali chloride salts, it avoids the generation of large volumes of acidic wastewater and hazardous organic solvent residues commonly associated with conventional hydrometallurgical routes [16].

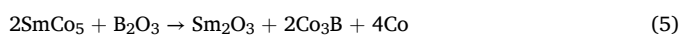
From the perspective of impurity management, the process selectivity arises from the different oxidation tendencies of rare-earth and transition-metal chlorides in the molten-salt environment. While Sm preferentially forms insoluble oxychloride phases, Co remains dissolved in the melt, thereby minimizing its incorporation into the precipitated Sm-rich product. This selective phase partitioning is essential for maintaining high Sm recovery and purity during oxidative precipitation [16]. This investigation focuses only on the separation of Sm and Co by oxygenation in LiCl-KCl melts; the effects of other elements present in Sm-Co magnets have not been investigated. Additionally, the actual behavior of Co, especially in the presence of real impurities from industrial waste, has not been studied. The exact reaction mechanism, the role of mass transfer, and the influence of parameters such as oxygen pressure and the precise melt composition have not been analyzed. The kinetic modeling is also limited to a simple apparent reaction order. Furthermore, the stability and detailed structure of the  $\text{SmOCl}$  phase, as well as particle size, and their impact on separation and filtration performance have not been investigated.

### 3.3. Glass slag method

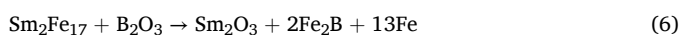
The glass slag method is a robust and effective approach for selectively extracting and separating Sm from REE-based alloys, particularly Sm-Co and Sm-Fe-N systems [45,46]. In this process, the bulk alloy is encapsulated in molten boron trioxide ( $\text{B}_2\text{O}_3$ ), which serves as both a reactive slag and a protective environment. The assembly is first slowly preheated to a temperature slightly above the slag's melting point to ensure complete coverage of the alloy by the molten glass. The system is maintained under an inert argon atmosphere to prevent oxidation and unwanted side reactions. Once the slag is fully molten, the alloy is superheated to temperatures well above its equilibrium liquidus: 1400 °C for  $\text{SmCo}_5$  and 1560 °C for  $\text{Sm}_2\text{Fe}_{17}\text{N}_3$ , thereby facilitating decomposition of the parent phases and promoting interfacial reactions between the alloy and the slag [45-47].

For Sm-Co alloys, the primary magnetic phases are  $\text{SmCo}_5$  and  $\text{Sm}_2\text{Co}_7$ . At elevated temperatures,  $\text{SmCo}_5$  decomposes into  $\text{Sm}_2\text{Co}_7$  and

Sm<sub>2</sub>Co<sub>17</sub>, but rapid cooling via metal mold casting prevents this decomposition, preserving the desired phase [41,42,47]. Upon immersion in molten B<sub>2</sub>O<sub>3</sub>, the Sm-Co alloy undergoes a reaction represented by Equ. 5. This reaction results in the formation of Co<sub>3</sub>B and metallic Co in the alloy. At the same time, Sm is transferred to the slag phase as Sm<sub>2</sub>O<sub>3</sub> and SmBO<sub>3</sub> [47]. B<sub>2</sub>O<sub>3</sub> is used in excess, typically at a 12-fold stoichiometric excess, to ensure complete extraction. This pyrometallurgical process yields a Co-B alloy with residual Sm content below 0.05% by mass. In contrast, Sm effectively partitions into the slag phase, achieving an enriched concentration that exceeds 58 mass% [46,47]. However, this slag should be regarded as an intermediate Sm-rich concentrate rather than a final recovered product; a potential downstream route would involve crushing the slag followed by acid leaching or acid baking-water leaching to dissolve Sm-bearing oxide/borate phases, with subsequent Sm recovery by precipitation or solvent extraction. The presence of Sm<sub>2</sub>Co<sub>7</sub> and SmCo<sub>5</sub> in the initial alloy can slightly alter the boron content in the final product, with measured values (3.0 wt%) marginally lower than the theoretical value (3.54 wt%) due to phase-composition effects [47].



In the case of Sm-Fe-N magnets, the dominant magnetic phase is Sm<sub>2</sub>Fe<sub>17</sub>N<sub>3</sub>, which is generated by nitriding Sm<sub>2</sub>Fe<sub>17</sub> alloys [45,46]. However, Sm<sub>2</sub>Fe<sub>17</sub>N<sub>3</sub> is thermally unstable above 600 °C and decomposes into α-Fe and Sm-N during the glass slag process. The Sm-N phase subsequently reacts with molten B<sub>2</sub>O<sub>3</sub> to form BN, while Sm is transferred to the slag phase. The overall reaction for Sm-Fe alloys can be seen as Equ. 6. The resulting Fe-B alloy contains less than 0.02 wt% Sm, while the slag phase is again enriched with Sm (51-58 wt%). The BN phase is detected in the slag, confirming the reaction pathway. The process effectively separates the challenging magnetic Sm<sub>2</sub>Fe<sub>17</sub>N<sub>3</sub> phase into a soft magnetic α-Fe phase and a Sm-rich slag, facilitating the extraction of Sm and the production of a magnetically soft material [45, 46]. The reported phase evolution further indicates that impurity separation in the glass slag method is governed by strong phase partitioning between the molten slag and the metallic alloy. Sm preferentially concentrates in the glassy slag phase, whereas transition metals such as Co and Fe remain predominantly in the metallic boride-rich alloy. This clear separation behavior contributes significantly to the high selectivity and low residual Sm content reported for the metallic phase [45,46].



Several gaps need to be addressed to deepen the understanding of this process. No thermodynamic or kinetic analysis has been presented. The effects of parameters such as temperature, residence time, heating and cooling rates, different B<sub>2</sub>O<sub>3</sub>-to-alloy ratios, particle size, sample geometry, and process atmosphere have not been examined. As a result, the method remains unoptimized for industrial applications. Most importantly, no approach has been proposed to recover Sm from the glass and return it to the material cycle. The influence of real impurities present in industrial waste has also not been investigated. Therefore, the major scientific and industrial steps (including clarification of mechanisms, process optimization, modeling, and final recycling) remain unaddressed and offer substantial opportunities for future research.

## 4. Integrated pyro-hydrometallurgical routes

### 4.1. Acid baking

Acid baking with nitric acid has been shown to be an effective route for selectively extracting Sm from Sm-Co PM scrap via controlled nitrate formation and thermal decomposition. In this method, Sm-Co magnet powders are first converted into a mixed nitrate system by reaction with concentrated nitric acid, yielding primarily Sm(NO<sub>3</sub>)<sub>3</sub>, Co(NO<sub>3</sub>)<sub>2</sub>, and Fe(NO<sub>3</sub>)<sub>3</sub>. The selectivity of the process arises from the fact that Sm nitrate

remains water-soluble at intermediate temperatures, while Co and Fe are converted to water-insoluble oxides [1,48]. Thermodynamic calculations using HSC Chemistry indicate that acid baking with nitric acid is energetically favorable over the temperature range 0-500 °C, with room temperature formation of nitrates being preferred on an energy basis [48]. When magnet powders are exposed to concentrated nitric acid, REEs, Fe, and Co participate in hydrogen- and nitric oxide-generating reactions of the type  $2\text{M} + 6\text{HNO}_3 \rightarrow 2\text{M}(\text{NO}_3)_3 + 3\text{H}_2\uparrow$  and  $\text{M} + 4\text{HNO}_3 \rightarrow \text{M}(\text{NO}_3)_3 + \text{NO}\uparrow + 2\text{H}_2\text{O}\uparrow$ . In this reaction, M represents REEs, Fe, or Co. Baking with nitric acid thus produces energetic nitrates Sm(NO<sub>3</sub>)<sub>3</sub>, Co(NO<sub>3</sub>)<sub>2</sub>, and Fe(NO<sub>3</sub>)<sub>3</sub> at room temperature, which can subsequently be decomposed in a controlled manner to achieve phase separation [1,48].

The thermal decomposition behaviors of Sm, Co, and Fe nitrates differ significantly and underpin the separation strategy. Sm nitrate hexahydrate (Sm(NO<sub>3</sub>)<sub>3</sub>•6H<sub>2</sub>O) initially dehydrates and passes through intermediate oxo-nitrate phases containing O-Sm-OH groups before fully decomposing to Sm oxide. In the temperature range 600-700 °C, the overall decomposition may be represented as  $2[\text{Sm}(\text{NO}_3)_3\bullet 6\text{H}_2\text{O}] \rightarrow \text{Sm}_2\text{O}_3 + 2\text{HNO}_3 + 4\text{NO}_2 + \text{O}_2 + 11\text{H}_2\text{O}$ . However, at lower temperatures around 250 °C, Sm(NO<sub>3</sub>)<sub>3</sub>•6H<sub>2</sub>O is only partially dehydrated. Therefore, the water content decreases, but the compound remains in nitrate form and retains its water solubility. In contrast, cobalt nitrate hexahydrate, Co(NO<sub>3</sub>)<sub>2</sub>•6H<sub>2</sub>O, undergoes a stepwise dehydration followed by conversion to Co oxides at substantially lower temperatures. The sequence of transformations is  $\text{Co}(\text{NO}_3)_2\bullet 6\text{H}_2\text{O} \rightarrow \text{Co}(\text{NO}_3)_2\bullet 4\text{H}_2\text{O} + 2\text{H}_2\text{O}$  at ~34 °C,  $\text{Co}(\text{NO}_3)_2\bullet 4\text{H}_2\text{O} \rightarrow \text{Co}(\text{NO}_3)_2\bullet 2\text{H}_2\text{O} + 2\text{H}_2\text{O}$  when temperature reaches around 67 °C, and  $\text{Co}(\text{NO}_3)_2\bullet 2\text{H}_2\text{O} \rightarrow \text{Co}(\text{NO}_3)_2 + 2\text{H}_2\text{O}\uparrow$  at ~110 °C. Subsequent decomposition of the anhydrous nitrate yields Co oxides via  $2\text{Co}(\text{NO}_3)_2 \rightarrow \text{Co}_2\text{O}_3 + \text{N}_2\text{O}_4 + \text{N}_2\text{O}_5$  and  $3\text{Co}(\text{NO}_3)_2 \rightarrow \text{Co}_3\text{O}_4 + \text{N}_2\text{O}_4 + 2\text{N}_2\text{O}_5$  at around 185 °C. Thermodynamic analysis indicates that the latter oxide-forming reaction is not feasible, with a Gibbs free energy of  $\Delta G = +188.905$  kJ at 185 °C, whereas the formation of Co<sub>3</sub>O<sub>4</sub> proceeds under the same conditions. Consequently, in practice, cobalt predominantly forms Co<sub>3</sub>O<sub>4</sub> [1].

Iron nitrate exhibits a distinct decomposition pathway that also leads to the formation of insoluble oxide. Hydrated iron nitrate, Fe(NO<sub>3</sub>)<sub>3</sub>•9H<sub>2</sub>O, first undergoes dehydration and nitrate release according to  $\text{Fe}(\text{NO}_3)_3\bullet 9\text{H}_2\text{O} \rightarrow \text{Fe}(\text{OH})(\text{NO}_3)_2\bullet 2\text{H}_2\text{O} + \text{HNO}_3\uparrow + 6\text{H}_2\text{O}\uparrow$  in the temperature range 50-100 °C. Further dehydration at approximately 105 °C yields Fe(OH)<sub>2</sub> through  $\text{Fe}(\text{OH})(\text{NO}_3)_2\bullet 2\text{H}_2\text{O} \rightarrow \text{Fe}(\text{OH})_2\text{NO}_3 + \text{HNO}_3\uparrow + \text{H}_2\text{O}\uparrow$ . With increasing temperature to around 150 °C, Fe(OH)<sub>2</sub>NO<sub>3</sub> transforms into goethite (FeOOH) via  $\text{Fe}(\text{OH})_2\text{NO}_3 \rightarrow \text{FeOOH} + \text{HNO}_3\uparrow$ . Finally, at approximately 400 °C, hematite is formed according to  $2\text{FeOOH} \rightarrow \text{Fe}_2\text{O}_3 + \text{H}_2\text{O}\uparrow$ . The contrasting decomposition profiles of Sm, Co, Fe nitrates thus demonstrate that controlled heating can be used to separate these metals. In this process, Sm remains in a water-soluble nitrate form at intermediate temperatures (~250 °C), while Co and Fe are present as water-insoluble oxides. Under integrated optimal conditions, acid baking at 250 °C for 2 h with an S/L of 1:5, followed by water leaching at an S/L of 1:10 for 2 h, results in Sm extraction exceeding 95%. At the same time, Co and Fe dissolution remain below 1%. The resulting leachate attains a REE purity of 99.4%, confirming the process's high selectivity. For environmental compliance and worker safety, the process is therefore implemented in a sealed reactor, where the generated NO<sub>x</sub> gases are captured and transferred to collection bottles rather than vented directly to the atmosphere [1].

As an alternative to conventional reactor heating, a solution-combustion route has also been investigated for converting Sm nitrate to Sm<sub>2</sub>O<sub>3</sub>. In this approach, Sm-Co magnet powders are reacted with nitric acid as before, but citric acid is added as a fuel. Subsequently, the mixture is subjected to solution combustion rather than isothermal baking. The reported Gibbs free energy profile suggests that the combustion reaction is thermodynamically favorable over the considered temperature range. The Gibbs free-energy profile was taken from the thermodynamic analysis of the stoichiometric solution-combustion

reaction between  $\text{Sm}(\text{NO}_3)_3$  and citric acid to form  $\text{Sm}_2\text{O}_3$ . The  $\Delta G$ -T trend was evaluated over approximately 0-500 °C under standard-state assumptions and was used only to assess thermodynamic feasibility rather than reaction kinetics. The overall response led to the formation of  $\text{Sm}_2\text{O}_3$ , as depicted schematically in the corresponding Gibbs energy-temperature diagram (Fig. 6). Citric acid was introduced in different fuel-to-oxidizer ratios ( $\phi$ ) to elucidate its influence on combustion behavior and product morphology. An increase in  $\phi$  from 0.5 to 2 resulted in progressively more intense combustion, accompanied by higher reaction temperatures and pronounced gas evolution, which, in turn, promoted the formation of highly agglomerated powders. At  $\phi = 0.5$ , the synthesized  $\text{Sm}_2\text{O}_3$  powders exhibited a relatively spherical surface morphology. In contrast, at  $\phi = 1$  and 2, the powders displayed irregular shapes and broad size distributions. The irregular and flaky particles were attributed to nonuniform temperature and mass-flow distributions within the combustion flame. Thus, while solution combustion offers a rapid route to  $\text{Sm}_2\text{O}_3$ , the choice of  $\phi$  strongly governs the product's microstructure and must be carefully controlled for applications where particle morphology is critical [48]. The exact kinetic behavior of the nitrate-to-oxide conversion has not been modeled, and the effects of parameters such as  $\text{NO}_x$  vapor pressure, humidity, and heating rate on the selectivity of Co/Fe oxidation over Sm have not been investigated. In the leaching section, the detailed dissolution mechanism of  $\text{Sm}(\text{NO}_3)_3$  and the effects of pH, temperature, and interfering ions have not been analyzed. Also, the study does not address the recovery or final separation of Co and Fe from the oxide residue. In addition, precise control of  $\text{Sm}_2\text{O}_3$  particle size, the mechanism of nanoparticle growth during combustion, and flame-reaction modeling have not been explored.

#### 4.2. Sulfation and selective oxidation

Sulfation is a pyrometallurgical method conducted at elevated temperatures in the presence of sulfur oxides, enabling selective oxidation and phase transformation of metal-bearing compounds. It provides an effective route in extractive metallurgy for metal separation and recovery. Time, temperature, and acid concentration are the primary variables controlling both the formation and decomposition of metal sulfates and oxy-sulfates. Therefore, these parameters must be precisely optimized to maximize REE extraction while suppressing undesired side reactions. For recovering Sm-Co magnet powders, sulfation and selective oxidation can be applied to extract and separate Sm, Co, Cu, and Fe. Initially, the powders are mixed with concentrated sulfuric acid (96%)

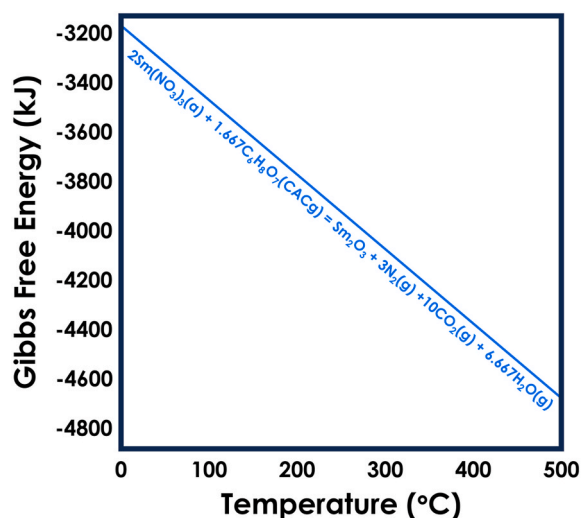


Fig. 6. Thermodynamic Gibbs free energy curve of the solution combustion process (Based on [48]).

to promote the conversion of most oxides into their corresponding sulfates. During subsequent selective oxidation in a muffle furnace, these sulfates, characterized by relatively low thermal stability, decomposed to water-insoluble oxides. This enables the separation of REEs from base metals in the subsequent water-leaching step. Iron sulfate phases first transformed to FeO when the temperature exceeded the stability range of Fe sulfates and then to  $\text{Fe}_2\text{O}_3$  through oxidation by atmospheric oxygen and/or via slow  $\text{SO}_3$  decomposition [2].

During the process, selective oxidation was designed to exploit the differences in thermal stability between REE sulfates and base-metal sulfates.  $\text{Sm}_2(\text{SO}_4)_3$  dehydrated (100-300 °C) and started decomposing near  $\sim 700$  °C. A strong mass-loss event occurred around  $\sim 800$  °C, with continued loss to  $\sim 890$  °C. Sm sulfate converted to  $\text{Sm}_2\text{O}_2(\text{SO}_4)$  (oxy-sulfate)  $\sim 900$  °C, then to  $\text{Sm}_2\text{O}_3$   $\sim 1210$  °C. Other REE sulfates could behave similarly:  $\text{R}_2(\text{SO}_4)_3 \rightarrow \text{R}_2\text{O}_2(\text{SO}_4) + \text{SO}_3(\text{g}) \rightarrow \text{R}_2\text{O}_3 + 2\text{SO}_3(\text{g})$ . For Nd/Pr, major decomposition is in a narrow window  $\sim 855$ - $946$  °C, forming largely water-insoluble  $\text{R}_2\text{O}_3$ . Below that window, REE sulfates remain relatively stable and water-soluble (suitable for later leaching). In contrast, Co/Cu/Fe sulfates decompose at lower temperatures, forming CoO/ $\text{Co}_3\text{O}_4$ , CuO, and  $\text{Fe}_2\text{O}_3$ , while REE sulfates persist. Thus, selective oxidation should be carried out at 650-800 °C to decompose base-metal sulfates while preserving Sm/Nd/Pr sulfates. Performance showed a clear threshold:  $\sim 750$  °C favors Sm sulfate formation (high recovery) with limited oxy-sulfate. At 800 °C, Sm recovery collapsed (Fig. 7) because Sm oxy-sulfate formed (water-insoluble), matching thermal gravimetric analysis (TGA) onset. Therefore, key pyrometallurgical controls were temperature (avoid  $\geq 800$  °C to prevent Sm sulfate retention) and time/acid loading to limit oxy-sulfate formation while fully oxidizing base metals [2]. Despite this method's technical potential, some gaps remain. The precise thermodynamic and kinetic behavior of the sulfation and oxidation steps has not been modeled, and the reaction mechanisms have only been reported experimentally. Furthermore, the effects of impurities, particle size, and the magnet's microcrystalline structure on separation efficiency have not yet been investigated.

Thermal processing routes such as nitric acid baking and sulfation roasting inherently generate  $\text{NO}_x$  and  $\text{SO}_x$ , requiring effective off-gas management to ensure environmental compliance and operational safety. Recent pilot-scale process designs have therefore incorporated dedicated gas-capture systems to minimize the direct atmospheric release of these hazardous species. In sulfation-based systems, sulfur oxides generated during sulfate decomposition can potentially be recovered and recycled for sulfuric acid production, supporting more integrated chemical utilization. Similarly,  $\text{NO}_x$  released during nitric acid baking may be regenerated into nitric acid through oxy-hydrolysis-based recovery systems, thereby reducing reagent consumption and environmental impact. Industrial emission-control technologies, including alkali scrubbing and catalytic reduction systems for  $\text{NO}_x$  conversion to  $\text{N}_2$ , are therefore important considerations for future scale-up and industrial implementation. The integration of such gas-treatment units could substantially improve the environmental sustainability of pyrometallurgical recycling flowsheets while simultaneously enabling partial recovery and reuse of process chemicals.

#### 4.3. Solid-state chlorination

The solid-state chlorination method employing  $\text{NH}_4\text{Cl}$  for  $\text{SmCo}_5$  magnet powder is grounded in rigorous thermodynamic and kinetic principles, making it a promising approach for efficient REE recovery [11].  $\text{NH}_4\text{Cl}$  decomposes at 338 °C into  $\text{NH}_3$  and HCl, with decomposition occurring more slowly at temperatures below 338 °C due to the equilibrium established between the two partial pressures of  $\text{NH}_3$  and HCl [49]. Notably, the slow release of HCl at temperatures between 225 °C and 325 °C extends the residence time for the HCl-gas reaction with  $\text{SmCo}_5$ , thereby enhancing the formation of metal chlorides and improving REE extraction efficiency. Similar optimization has been observed for  $\text{Fe}_{14}\text{Nd}_2\text{B}$  magnets, where chlorination is most effective

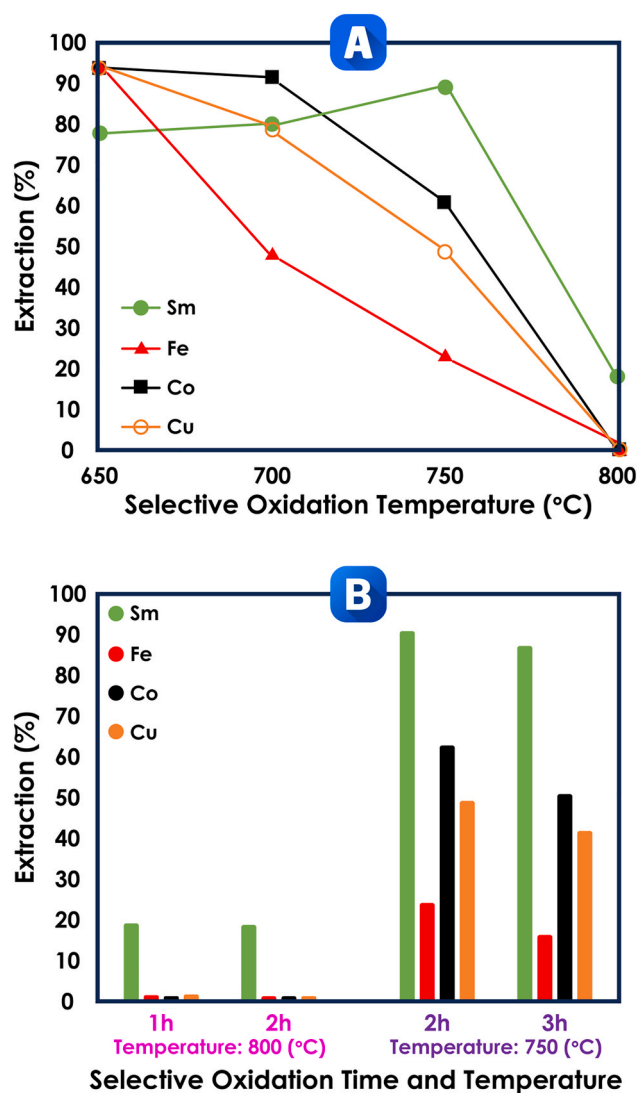
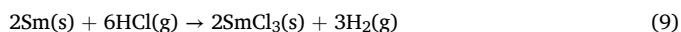
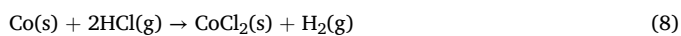


Fig. 7. Extraction behavior of Sm, Fe, Co, and Cu during sulfation and selective oxidation process. (A) Effect of oxidation temperature and (B) influence of oxidation time at 750 °C and 800 °C (Based on [2]).

within this temperature range [11].

The key solid-state reactions are as follows:



The feasibility of these reactions is determined by the Gibbs free energy change  $\Delta G$ .  $\text{NH}_4\text{Cl}$  decomposition (Reaction 7) has a slightly positive  $\Delta G$  of +7.170 kJ at lower temperatures, becomes negative (−0.248 kJ) at ~367 °C, and becomes more favorable (−18.241 kJ) only above 438 °C. Chlorination of Co and Sm (Reactions 8 and 9) is thermodynamically favorable across the operating temperatures, with  $\Delta G$  values at 225 °C of −47.597 kJ for Co and −611.910 kJ for Sm, and at 325 °C of −32.742 and −585.446, respectively. The markedly more negative  $\Delta G$  for Sm reflects its tendency toward preferential, robust chlorination under these conditions. In the rotary-kiln chlorination route,  $\text{NH}_4\text{Cl}$  was thermally decomposed to generate in situ HCl, thereby converting Sm and Co into water-soluble chlorides. At the same time, off-gases ( $\text{H}_2$ ,  $\text{N}_2$ ,  $\text{NH}_3$ , and excess HCl) were continuously removed and subsequently treated (cooling to <200 °C to recombine  $\text{NH}_3/\text{HCl}$ ,  $\text{NH}_3$

scrubbing, and  $\text{H}_2$  combustion). Temperature is the dominant pyrometallurgical lever, followed by residence time: higher temperature accelerates chlorination, but lower  $\text{NH}_4\text{Cl}$  dosing at high temperature can strongly increase Sm selectivity, since Co chlorination is more sensitive to  $\text{NH}_4\text{Cl}$  mass. A key selective condition reported was 325 °C with ~0.5 g/g  $\text{NH}_4\text{Cl}$ , giving ~99% Sm recovery while keeping Co recovery low (~20%), leaving most Co unreacted. Conversely, higher  $\text{NH}_4\text{Cl}$  loadings (e.g., ~3 g (per gram magnet) at 325 °C for longer times) could promote co-chlorination and increase Co recovery to ~70%. Reaction progress was also reflected morphologically: chlorination formed a RE-chloride layer/shell, and for  $\text{SmCo}_5$ , a robust chloride shell disaggregated from the core into fine particles, aiding downstream separation of chlorinated RE products [11]. For further development of this technique, several avenues remain for future research. A detailed thermodynamic and kinetic analysis of chlorination reactions has not been provided, and the modeling relies only on the design of experiments without quantitatively examining the reaction mechanism, reaction rates, or the role of intermediate phases. The effects of particle size, surface oxidation, and real Sm-Co compositions (such as  $\text{Sm}_2\text{Co}_{17}$ ) have not been systematically investigated, and the process stability with respect to variations in feed composition remains uncertain. Table 2 lists the pyrometallurgical and integrated recycling routes for Sm-Co magnets, together with their operating conditions, major advantages, limitations, and performances.

## 5. Thermal processing of hydro products

Following the application of various processing techniques, the recovery of secondary resources often yields products in the form of ionic species in solution or as solid compounds such as nitrates, carbonates, or oxalates [17,48,50,51]. The removal of residual organic impurities derived from metallurgical processes or precipitation and the transformation of intermediates into stable, storable, and marketable solids represent essential stages in the refining process [3,44,52]. The final step, typically involving calcination, aims to generate crystalline oxides that can be readily reintegrated into production lines [12,20,48,52]. Metal oxides are often favored as terminal products due to their superior thermodynamic stability at elevated temperatures commonly used during heat treatments [1,3,48]. This stability arises from their high lattice energies and strongly negative Gibbs free energies of formation ( $\Delta G_f^\circ$ ), making their further decomposition energetically unfavorable [3,53]. Such thermodynamic considerations are particularly relevant for REEs such as Sm and transition metals such as Co, whose oxides ( $\text{Sm}_2\text{O}_3$  and  $\text{Co}_3\text{O}_4$ ) exhibit robust structural and chemical durability [12,54].

Calcination is therefore a critical step in the recovery of Sm-Co magnets and related materials. It ensures not only purity and structural integrity but also operational simplicity and cost-effectiveness [12, 52,55]. Across numerous studies, the conversion of Sm oxalate precipitates obtained from reactions involving  $\text{Sm}^{3+}$  ions and oxalic acid or sodium oxalate has been performed at 800–950 °C for approximately 1–2 h, usually in a temperature-controlled muffle furnace [15,21,43,52, 55]. Following filtration and washing, commonly with distilled water and occasionally with isopropyl alcohol, this treatment yields high-purity  $\text{Sm}_2\text{O}_3$  [43,52]. The high purity of the final products has been confirmed by XRD analyses, which show complete agreement with reference patterns [21,43,52]. Alternatively, Sm hydroxide [ $\text{Sm}(\text{OH})_3$ ], formed through the reaction of NaOH with  $\text{NaSm}(\text{SO}_4)_2$ , has been thermally treated at 800 °C for 120 min to produce cubic  $\text{Sm}_2\text{O}_3$  with particle sizes near 50 nm and purity reaching 99.5%. In this method, NaOH consumption was estimated at 0.26 kg per kilogram of  $\text{Sm}_2\text{O}_3$  [15]. Although highly efficient, this hydroxide route is more reagent-intensive than oxalic-based pathways, which can yield comparable results using less chemical input [15,48,52].

Co recovery follows a similar thermal strategy, but at lower temperatures because of the distinct stability of its precursor compounds [12]. In most reports, Co oxalate ( $\text{CoC}_2\text{O}_4$ ) is calcined at 400–500 °C for

**Table 2**  
Comparative summary of the main pyrometallurgical and hydro-pyrometallurgical recycling routes for Sm-Co magnets.

Process	Main Principle	Operating Conditions	Main Advantages	Main Limitations	Reported Recovery/Selectivity
Vacuum Distillation	Selective Sm evaporation under high vacuum based on vapor pressure differences	<ul style="list-style-type: none"> <li>● ~1300-1500 °C.</li> <li>● ~8 × 10<sup>-3</sup> Pa vacuum.</li> </ul>	<ul style="list-style-type: none"> <li>● High Sm selectivity.</li> <li>● No aqueous waste.</li> <li>● High-purity of Sm.</li> <li>● Suitable for impurity-tolerant feeds.</li> </ul>	<ul style="list-style-type: none"> <li>● Very high temperature.</li> <li>● Cu co-evaporation at elevated temperatures.</li> <li>● Condenser-material sensitivity.</li> <li>● High energy demand.</li> <li>● Limited industrial validation.</li> <li>● Influence of impurities is insufficiently studied.</li> <li>● High-temperature salt handling required.</li> </ul>	<ul style="list-style-type: none"> <li>● Sm enrichment &gt;95% using Mo condenser.</li> <li>● Sm purity &gt;99% below 1400 °C but decreased to ~85.24% at higher temperature because of Cu volatilization.</li> <li>● SmOCl selectively formed while Co remained dissolved.</li> <li>● ΔG for SmOCl formation = -67.8 kJ/mol at 700 °C.</li> </ul>
Molten Salt Extraction (LiCl-KCl)	Selective oxidation of Sm chloride to insoluble SmOCl in molten salt	<ul style="list-style-type: none"> <li>● ~400-700 °C.</li> <li>● LiCl-KCl eutectic.</li> <li>● Oxygen sparging.</li> </ul>	<ul style="list-style-type: none"> <li>● Reusable molten medium.</li> <li>● High thermodynamic selectivity.</li> <li>● Lower wastewater generation.</li> <li>● Possibility of electrochemical salt regeneration.</li> </ul>	<ul style="list-style-type: none"> <li>● High thermal demand.</li> <li>● No complete downstream Sm recovery strategy from slag.</li> <li>● Limited process optimization studies.</li> </ul>	<ul style="list-style-type: none"> <li>● Metallic alloy contained &lt;0.05 wt% Sm.</li> <li>● Slag enriched with &gt;58 wt% Sm.</li> </ul>
Glass Slag Method	Transfer of Sm into molten B <sub>2</sub> O <sub>3</sub> slag while Co/Fe form metallic boride phases	<ul style="list-style-type: none"> <li>● ~1400 °C.</li> <li>● Inert atmosphere.</li> <li>● Excess B<sub>2</sub>O<sub>3</sub>.</li> </ul>	<ul style="list-style-type: none"> <li>● Efficient Sm partitioning.</li> <li>● Very low residual Sm in metallic alloy.</li> <li>● Effective separation of metallic phases.</li> </ul>	<ul style="list-style-type: none"> <li>● Generates NO<sub>x</sub> gases.</li> <li>● Requires gas-treatment systems.</li> <li>● Acid consumption.</li> </ul>	<ul style="list-style-type: none"> <li>● Sm extraction &gt;95%.</li> <li>● Co and Fe dissolution &lt;1%.</li> <li>● REE purity ~99.4%.</li> </ul>
Nitric Acid Baking	Formation and controlled decomposition of metal nitrates followed by selective water leaching	<ul style="list-style-type: none"> <li>● ~250 °C baking.</li> <li>● ~2 h.</li> <li>● HNO<sub>3</sub> treatment.</li> <li>● Water leaching.</li> </ul>	<ul style="list-style-type: none"> <li>● Very high Sm selectivity.</li> <li>● Relatively low thermal requirement.</li> <li>● High REE purity.</li> <li>● Good selectivity between REEs and base metals.</li> <li>● Suitable for integrated pyro-hydro systems.</li> </ul>	<ul style="list-style-type: none"> <li>● SO<sub>x</sub> generation.</li> <li>● Narrow optimal. Temperature window.</li> <li>● Sm oxy-sulfate formation above ~800 °C reduces recovery.</li> </ul>	<ul style="list-style-type: none"> <li>● High Sm sulfate stability below ~800 °C.</li> <li>● Recovery sharply decreased at excessive temperature because of oxy-sulfate formation.</li> </ul>
Sulfation and Selective Oxidation	Sulfate formation followed by the selective decomposition of base-metal sulfates	<ul style="list-style-type: none"> <li>● ~650-800 °C.</li> <li>● Concentrated H<sub>2</sub>SO<sub>4</sub>.</li> </ul>	<ul style="list-style-type: none"> <li>● High Sm selectivity.</li> <li>● Relatively moderate temperature.</li> <li>● Promotes particle disintegration.</li> </ul>	<ul style="list-style-type: none"> <li>● Requires gas handling for NH<sub>3</sub>/HCl/H<sub>2</sub>.</li> <li>● Feed-composition sensitivity.</li> <li>● Kinetic mechanisms insufficiently understood.</li> </ul>	<ul style="list-style-type: none"> <li>● ~99% Sm recovery with limited Co chlorination under optimized conditions.</li> </ul>
Solid-State Chlorination	NH <sub>4</sub> Cl decomposition generates HCl for the selective chlorination of Sm	<ul style="list-style-type: none"> <li>● ~225-325 °C.</li> <li>● NH<sub>4</sub>Cl chlorination.</li> <li>● Rotary kiln.</li> </ul>	<ul style="list-style-type: none"> <li>● High Sm selectivity.</li> <li>● Relatively moderate temperature.</li> <li>● Promotes particle disintegration.</li> </ul>	<ul style="list-style-type: none"> <li>● Requires gas handling for NH<sub>3</sub>/HCl/H<sub>2</sub>.</li> <li>● Feed-composition sensitivity.</li> <li>● Kinetic mechanisms insufficiently understood.</li> </ul>	<ul style="list-style-type: none"> <li>● ~99% Sm recovery with limited Co chlorination under optimized conditions.</li> </ul>

1-4 h to form Co<sub>3</sub>O<sub>4</sub> [12,51,52]. The morphological features of Co<sub>3</sub>O<sub>4</sub> obtained under these conditions generally include prismatic or rod-like particles (36 nm to 2 μm) at 1 h, which evolve into more regular, crystalline structures with longer calcination times. After 4 h, Co reaches a particle size of 49 nm [12,18]. Comparable trends are observed for Sm oxidation, where Sm<sub>2</sub>O<sub>3</sub> initially forms as agglomerated clusters at shorter calcination times (1 h). With increasing time and temperature, these clusters gradually develop into plate-like and spherical morphologies (2-5 μm, reaching 3-5 μm at 800 °C for 1-4 h, or 41-48 nm at 800 °C for 1-6 h). The observed enhancement in crystallinity has been attributed to an increase in particle size, which leads to larger volume-to-surface ratios, promotes internal atomic rearrangements, and favors ordered lattice formation [18].

Variations in thermal treatment parameters reflect the influence of precursor type and target metal oxide on process optimization. For instance, Deng et al. (2022) reported applying 950 °C for 2 h to ensure complete conversion of oxalate intermediates and to prepare the resulting oxides for selective separation in acetate-based media [55]. Conversely, Emil-Kaya et al. (2024) observed that Fe(NO<sub>3</sub>)<sub>3</sub>•9H<sub>2</sub>O decomposed to Fe<sub>2</sub>O<sub>3</sub> at a significantly lower temperature of 200 °C, revealing the precursor-dependent nature of calcination requirements [1]. Additional studies employing different precipitation agents, such as sodium oxalate and ammonium oxalate, demonstrate that Sm<sub>2</sub>(C<sub>2</sub>O<sub>4</sub>)<sub>3</sub> and CoC<sub>2</sub>O<sub>4</sub> can be efficiently transformed into Sm<sub>2</sub>O<sub>3</sub> and Co<sub>3</sub>O<sub>4</sub> under optimized conditions (800 °C for 1-6 h and 450 °C for 1-4 h, respectively) [18,56]. Extended calcination times for Sm (up to 6 h) and Co (up to 4 h) have been correlated with greater phase purity and improved

lattice order [18]. In another system involving ionic liquids, the oxalate precipitates of Sm<sup>3+</sup> and Co<sup>2+</sup> ions yielded an Sm<sub>2</sub>O<sub>3</sub> recovery of 83.9%, slightly lower than the >95% yields reported under other solvent or reagent conditions, suggesting extractant-dependent efficiency [20,43,56]. Table 3 summarizes the thermal processes applied to metal-bearing products for the production of final Co and REE oxide materials.

## 6. Summary

Sm and Co are critical raw materials for producing Sm-Co permanent magnets and are highly valued for their high thermal stability and corrosion resistance. These magnets are widely used in aerospace, defense, and high-temperature automotive industries. The growing demand for these technologies highlights the importance of recovering Sm-Co from secondary sources. The production of these magnets generates significant waste, and they contain a high concentration of valuable metals, making recycling economically and environmentally important. Recycling approaches used so far include hydrometallurgy and pyrometallurgy. Hydrometallurgy produces high-purity products but consumes a lot of chemicals, while pyrometallurgy offers high throughput and greater impurity tolerance. Thermal techniques play a crucial supporting role in hydrometallurgy, extending beyond pure pyrometallurgy, by enabling pre-treatment, facilitating integrated pyro-hydro processes, and enhancing final product processing.

Thermal demagnetization is the first major step in processing Sm-Co magnet waste, in which the material is heated to temperatures near or above its blind point, disrupting magnetic domains, breaking up particle

**Table 3**  
Summary of thermal processing conditions and details on Sm- and Co-bearing products.

Material	Temp. (°C)	Time (Hour)	Furnace Type	Final Product	Reported Purity	Test Repetition	Remarks	Ref.
Sm(OH) <sub>3</sub> Obtained from NaSm(SO <sub>4</sub> ) <sub>2</sub>	800	2	N.R.	Sm <sub>2</sub> O <sub>3</sub>	Sm recovery: 99.2% Sm <sub>2</sub> O <sub>3</sub> Purity: 99.5% CuSO <sub>4</sub> : >98%	N.R.	<ul style="list-style-type: none"> <li>●Sm<sub>2</sub>O<sub>3</sub> powder primary particle size ~50 nm.</li> <li>●NaOH consumption per kilogram of the Sm-Co swarf: 0.26 kg kg<sup>-1</sup>.</li> <li>●NaOH consumption per kilogram the yield of Sm<sub>2</sub>O<sub>3</sub>: 0.28 kg kg<sup>-1</sup>.</li> <li>●Particle size of Sm(OH)<sub>3</sub>: ~200 nm.</li> </ul>	[15]
Sm <sub>2</sub> (C <sub>2</sub> O <sub>4</sub> ) <sub>3</sub> Obtained from Na <sub>2</sub> C <sub>2</sub> O <sub>4</sub>	800	2	N.R.	Sm <sub>2</sub> O <sub>3</sub>	Sm <sub>2</sub> O <sub>3</sub> Purity: 99% The purity of Co in solution (CoCl <sub>2</sub> ): 99.5% Co recovery: 99%	N.R.	<ul style="list-style-type: none"> <li>●Roasted after precipitation and washing (3× with 4% NH<sub>3</sub>.H<sub>2</sub>O).</li> </ul>	[21]
Sm <sub>2</sub> (C <sub>2</sub> O <sub>4</sub> ) <sub>3</sub> Obtained from Na <sub>2</sub> C <sub>2</sub> O <sub>4</sub>	800	N.R.	Muffle Furnace	Sm <sub>2</sub> O <sub>3</sub>	Sm <sub>2</sub> O <sub>3</sub> Purity: 99.9% Co purity in Sm <sub>2</sub> O <sub>3</sub> : 0.02% Co chloride purity in raffinate: 95.14% Co recovery: 98.61%	N.R.	<ul style="list-style-type: none"> <li>●After stripping with Na<sub>2</sub>C<sub>2</sub>O<sub>4</sub>, the loaded organic phase was washed 3× with 4% NH<sub>3</sub>.H<sub>2</sub>O solution and calcined.</li> </ul>	[20]
Sm <sub>2</sub> (C <sub>2</sub> O <sub>4</sub> ) <sub>3</sub> Obtained from Na <sub>2</sub> C <sub>2</sub> O <sub>4</sub>	800	1	N.R.	Sm <sub>2</sub> O <sub>3</sub>	Highly Pure	N.R.	<ul style="list-style-type: none"> <li>●Precipitated with Na<sub>2</sub>C<sub>2</sub>O<sub>4</sub>, settled for 4 h, filtered, washed with distilled water, and dried before calcination.</li> <li>●Average crystalline size of Sm<sub>2</sub>O<sub>3</sub> particles: 35 nm.</li> <li>●Sm oxide consists of nearly spherical particles that are agglomerated, forming clusters.</li> </ul>	[43]
CoC <sub>2</sub> O <sub>4</sub> Obtained from Na <sub>2</sub> C <sub>2</sub> O <sub>4</sub>	450	1	N.R.	Co <sub>3</sub> O <sub>4</sub>	Pure	N.R.	<ul style="list-style-type: none"> <li>●Obtained from raffinate after Sm extraction, precipitated as an oxalate, filtered, oven dried, and calcined.</li> <li>●The average grain size of Co<sub>3</sub>O<sub>4</sub> particles: 36 nm.</li> <li>●Irregular morphology of Co<sub>3</sub>O<sub>4</sub> nanoparticles of different sizes.</li> </ul>	[43]
CoC <sub>2</sub> O <sub>4</sub> Obtained from oxalic acid	450	1	N.R.	Co <sub>3</sub> O <sub>4</sub>	Highly Pure	N.R.	<ul style="list-style-type: none"> <li>●The nanoparticles aggregate to adopt rod shapes.</li> <li>●Needle-like morphology for Co<sub>3</sub>O<sub>4</sub>.</li> <li>●After Sm extraction from the leach liquor, the raffinate contained Co. The precipitate was washed with water, dried, and calcined.</li> </ul>	[52]
Sm <sub>2</sub> (C <sub>2</sub> O <sub>4</sub> ) <sub>3</sub> Obtained from oxalic acid	800	1	N.R.	Sm <sub>2</sub> O <sub>3</sub>	Highly Pure	N.R.	<ul style="list-style-type: none"> <li>●Rod-shaped morphology (0.9 × 0.5 μm).</li> <li>●Filtered, washed repeatedly with water, and finally with isopropyl alcohol to remove organic impurities.</li> </ul>	[52]
NaSm(SO <sub>4</sub> ) <sub>2</sub> .H <sub>2</sub> O and then Sm <sub>2</sub> (C <sub>2</sub> O <sub>4</sub> ) <sub>3</sub> Obtained from Na <sub>2</sub> SO <sub>4</sub> and then oxalic acid	800	1	Muffle Furnace	Sm <sub>2</sub> O <sub>3</sub>	Highly Pure	N.R.	<ul style="list-style-type: none"> <li>●REEs precipitate as a double sulfate with anhydrous Na<sub>2</sub>SO<sub>4</sub>, allowing easy separation from the leach liquor by filtration.</li> <li>●Sm<sub>2</sub>(C<sub>2</sub>O<sub>4</sub>)<sub>3</sub> Precipitation by oxalic acid.</li> </ul>	[54]
Rare Earth Oxalate Obtained from oxalic acid	N.R.	N.R.	N.R.	Rare Earth Oxides	Sm <sub>2</sub> O <sub>3</sub> Purity: 83.92% Gd <sub>2</sub> O <sub>3</sub> Purity: 16.08%	N.R.	<ul style="list-style-type: none"> <li>●Precipitated with oxalic acid, filtered and washed, the filtrates were combined, and the precipitate was calcined to obtain oxides.</li> <li>●Added ammonium oxalate to the filtrate; the resulting precipitate was washed, dried, and roasted to yield rare earth oxides.</li> </ul>	[17]
Co(OH) <sub>3</sub> Obtained from hydroxide precipitation	N.R.	N.R.	N.R.	Cobalt Oxide	Co: 72.18 wt% Impurities: Fe, Sm, Gd, Cu, Zr <0.06%	N.R.	<ul style="list-style-type: none"> <li>●High-temperature calcination</li> <li>●The precipitate of Co(OH)<sub>3</sub> and Fe(OH)<sub>3</sub> was dissolved in hydrochloric acid (1 mol/L). By controlling the pH below 3.5, Fe(OH)<sub>3</sub> was preferentially dissolved, while Co(OH)<sub>3</sub> remained undissolved at pH above 1.4, enabling their separation.</li> </ul>	[17]
Metal Oxalate Obtained from oxalic acid	950	2	Air Furnace	Metal Oxides (Sm, Co, Cu oxides)	N.R.	N.R.	<ul style="list-style-type: none"> <li>●purification process; calcined oxides are later dissolved in acetic acid for extraction.</li> </ul>	[55]
Sm and Co Oxalates (IL-based) Obtained from ammonium oxalate	800	N.R.	N.R.	Sm <sub>2</sub> O <sub>3</sub>	Highly Pure	N.R.	<ul style="list-style-type: none"> <li>●Yield: 83.9%</li> </ul>	[56]
Sm(H <sub>2</sub> O) <sub>4</sub> (NO <sub>3</sub> ) <sub>3</sub> (H <sub>2</sub> O) and then Sm <sub>2</sub> (C <sub>2</sub> O <sub>4</sub> ) <sub>3</sub> Obtained from HNO <sub>3</sub> and then oxalic acid	N.R.	N.R.	N.R.	Sm <sub>2</sub> O <sub>3</sub>	N.R.	N.R.	<ul style="list-style-type: none"> <li>●Cubic structure of Sm<sub>2</sub>O<sub>3</sub></li> <li>●Rod-like shape</li> </ul>	[1]

agglomerates, and oxidizing to more reactive oxides. This transformation eliminates magnetic behavior and increases the efficiency of subsequent steps. Since Sm-Co alloys have strong magnetic-crystalline anisotropy, they require prolonged exposure to high temperatures (typically 800–900 °C) to achieve diamagnetism and complete oxidation.

Several pyrometallurgical routes have been developed for the selective recovery of Sm and Co. Vacuum distillation exploits Sm's much higher vapor pressure, enabling evaporation under high vacuum at temperatures above 1300 °C. Careful temperature control and selection of the condenser material (Mo is most effective) allow recovery of high-purity Sm and minimize co-evaporation of impurities. Another approach involves molten salt extraction using eutectic LiCl-KCl melts. In this process,  $\text{SmCl}_3$  readily converts to  $\text{SmOCl}$  or  $\text{Sm}_2\text{O}_3$  upon the introduction of oxygen. While Co chloride remains largely inactive. This thermodynamic selectivity provides a clean separation route in which the reaction rate is strongly influenced by temperature and Sm concentration. The glass slag method offers another route in which Sm-Co alloys are immersed in molten  $\text{B}_2\text{O}_3$ , transferring Sm to the slag as oxides and borates. On the other hand, Co or Fe forms metallic and boride phases. This process helps achieve high Sm enrichment in the slag (effectively separating Sm from both Sm-Co and Sm-Fe-N magnetic systems).

The overall efficiency of pyrometallurgical recovery is strongly influenced by the compositional and structural differences between  $\text{SmCo}_5$  and  $\text{Sm}_2\text{Co}_{17}$  alloys. In general,  $\text{SmCo}_5$  exhibits simpler phase behavior and higher selectivity during thermal processing. For example,  $\text{SmCo}_5$  particles readily undergo structural disintegration during solid-state chlorination, facilitating selective Sm extraction. In contrast,  $\text{Sm}_2\text{Co}_{17}$  alloys contain additional alloying elements such as Fe and Cu, which introduce greater process complexity and impurity-related selectivity challenges. This effect is particularly evident during vacuum distillation, where Cu co-evaporation at elevated temperatures can reduce Sm purity. Similar composition-dependent behavior is also observed in the glass slag method, where  $\text{SmCo}_5$  alloys typically form a distinct Sm-rich slag and Co-B alloy phase, whereas  $\text{Sm}_2\text{Co}_{17}$  systems generate more complex Fe-containing metallic phases.

Integrated pyro-hydrometallurgical systems improve selectivity. Acidic baking with nitric acid converts magnetic powders into mixed nitrates. During the heating step, Sm nitrate, Co, and Fe each decompose at different temperatures and in different ways. At about 250 °C, Co and Fe are converted into insoluble oxides, while Sm nitrate remains soluble in water, enabling selective Sm leaching with minimal contamination. A type of solution combustion can also produce  $\text{Sm}_2\text{O}_3$ , with particle morphology depending on the fuel ratio. Sulphation, followed by selective oxidation, enables a different thermal separation route. In this process, metal oxides are first converted to sulfates using concentrated sulfuric acid. Oxidation is conducted at a controlled temperature between 650 and 800 °C, decomposing the base-metal sulfates while retaining the REE sulfates. If the temperature exceeds this range, Sm oxysulfate is formed, which is insoluble in water and reduces recovery. Therefore, temperature control is a key factor. Solid-state chlorination with  $\text{NH}_4\text{Cl}$  relies on the slow release of HCl (225–325 °C) and enables selective chlorination of Sm and Co. Under optimal conditions, Sm is almost completely converted to  $\text{SmCl}_3$ , while the Co remains intact. The resulting chloride layers help to break down the particles for easier downstream processing. Finally, the oxalates, hydroxides, or nitrates are converted to stable, high-purity oxides. Sm oxalate is usually calcined at 800 °C to obtain  $\text{Sm}_2\text{O}_3$ , while Co oxalate requires a lower temperature of 400 to 500 °C to form  $\text{Co}_3\text{O}_4$ . These oxides have a strong structure and are thermodynamically stable, making them ideal for magnet production or other industrial applications.

#### CRedit authorship contribution statement

**Mehrdad Gharavi:** Investigation, Software, Visualization, Writing –

original draft, Writing – review & editing. **Sara Karimi Moghadam:** Investigation, Software, Visualization, Writing – original draft, Writing – review & editing. **Ali Asimi Neisiani:** Data curation, Investigation, Methodology, Project administration, Validation, Visualization, Writing – review & editing. **Carina Ulsen:** Investigation, Validation, Writing – review & editing. **Saeed Chehreh Chelgani:** Conceptualization, Methodology, Supervision, Writing – review & editing.

#### Declaration of competing interest

The authors declare that they have no known competing financial interests or personal relationships that could have appeared to influence the work reported in this paper.

#### Data availability

Data will be made available on request.

#### References

- [1] E. Emil-Kaya, X. Lu, B. Friedrich, Recovery of samarium and cobalt/iron oxide from SmCo magnets through acid baking and water leaching, *J. Mater. Cycles Waste Manag.* (2024) 3905–3916, <https://doi.org/10.1007/s10163-024-02096-1>.
- [2] M. Papakci, E. Emil-Kaya, S. Stopic, S. Gurmen, B. Friedrich, Recovery of valuable metals from SmCo magnets through sulfation, selective oxidation, and water leaching, *Separ. Sci. Technol.* 59 (2024) 1241–1254, <https://doi.org/10.1080/01496395.2024.2368229>.
- [3] Y.V. Murty, M.A. Alvin, J. Lifton, *Rare Earth Metals and Minerals Industries, Status and Prospects*, Springer Int. Publ., 2024, <https://doi.org/10.1007/978-3-031-31867-2>.
- [4] S. Ni, J. Su, H. Zhang, Z. Zeng, H. Zhi, X. Sun, A cleaner strategy for comprehensive recovery of waste SmCo magnets based on deep eutectic solvents, *Chem. Eng. J.* 412 (2021) 128602, <https://doi.org/10.1016/J.CEJ.2021.128602>.
- [5] S. Papagianni, A.M. Moschovi, K.M. Sakkas, M. Chalaris, I. Yakoumis, Preprocessing and leaching methods for extraction of REE from permanent magnets: a scoping review, *Appl. Chem.* 2 (2022) 199–212, <https://doi.org/10.3390/appliedchem2040014>.
- [6] C. Fang, Z. Yan, X.J. Zhang, F. Wang, X.H. Xu, Enhanced structural stability and magnetism of SmCo<sub>3</sub> permanent magnet doped with 3d transition metals: an Ab initio study, *Rare Met.* 44 (2) (2024), <https://doi.org/10.1007/S12598-024-02983-4>, 2024, 44, 1256–1266.
- [7] J. Croat, J. Ormerod (Eds.), *Modern Permanent Magnets*, Elsevier, 2022. ISBN 978-0-323-88658-1.
- [8] X. Xu, S. Khoshima, M. Karajic, J. Balderman, K. Markovic, J. Scancar, Z. Samardzija, S. Sturm, K.Z. Rozman, Electrochemical routes for environmentally friendly recycling of rare-earth-based (Sm–Co) permanent magnets, *J. Appl. Electrochem.* 52 (2022) 1081–1090, <https://doi.org/10.1007/s10800-022-01696-9>.
- [9] Y. Ghorbani, I.M.S.K. Ilankoon, N. Dushyantha, G.T. Nwaila, Rare Earth permanent magnets for the green energy transition: bottlenecks, current developments and cleaner production solutions, *Resour. Conserv. Recycl.* 212 (2025) 107966, <https://doi.org/10.1016/J.RECONREC.2024.107966>.
- [10] C. Fang, Z. Yan, X. Zhang, J. Xiao, F. Wang, X. Xu, First-principles study of structural stability and magnetic properties of Sm<sub>2</sub>Co<sub>17</sub> rare Earth permanent magnets doped with transition metal elements, *J. Rare Earths* 43 (2025) 2682–2689, <https://doi.org/10.1016/J.JRE.2024.10.006>.
- [11] T. Lorenz, M. Bertau, Recycling of rare Earth elements from SmCo<sub>5</sub>-Magnets via solid-state chlorination, *J. Clean. Prod.* 246 (2020) 118980, <https://doi.org/10.1016/J.JCLEPRO.2019.118980>.
- [12] M.K. Sinha, S. Pramanik, A. Kumari, S.K. Sahu, L.B. Prasad, M.K. Jha, K. Yoo, B. D. Pandey, Recovery of value added products of Sm and Co from waste SmCo magnet by hydrometallurgical route, *Sep. Purif. Technol.* 179 (2017) 1–12, <https://doi.org/10.1016/j.seppur.2017.01.056>.
- [13] O. Chandrow, Rare Earth elements: a global scenario and understanding of their impacts, challenges, and recycling processes in Bangladesh through global literature, *대한환경공학회지* 46 (2024) 498–517, <https://doi.org/10.4491/KSEE.2024.46.9.498>.
- [14] S. Chehreh Chelgani, A. Asimi Neisiani, *Dry Mineral Processing*, Springer Nature, 2022. ISBN 978-3-030-93750-8.
- [15] X. Xu, J. Gao, K. Zhao, H. Sun, P. Jing, B. Liu, J. Zhang, A cleaner strategy for efficient recovery of Sm<sub>2</sub>O<sub>3</sub> and CoFeCu alloy from SmCo swarf based on an anodic leaching process, *Green Chem.* 26 (2024) 2552–2559, <https://doi.org/10.1039/D3GC04679F>.
- [16] D. Maltsev, P.W. Halstenberg, S.M. Mahurin, S. Dai, Promising method of Sm-Co magnet reprocessing in alkali chloride melts, *Ind. Eng. Chem. Res.* 61 (2022) 16577–16583, <https://doi.org/10.1021/acs.iecr.2c02682>.
- [17] T. Xu, X. Zhang, Z. Lin, B. Lü, C. Ma, X. Gao, Recovery of rare Earth and cobalt from Co-Based magnetic scraps, *J. Rare Earths* 28 (2010) 485–488, [https://doi.org/10.1016/S1002-0721\(10\)60355-9](https://doi.org/10.1016/S1002-0721(10)60355-9).

- [18] N. Swain, S. Mishra, Synthesis of nanosized Sm and Co oxides by liquid–liquid extraction scheme and investigation into separation chemistry employing tri-alkyl phosphine oxide as an extractant, *Chem. Pap.* 76 (2022) 945–959, <https://doi.org/10.1007/s11696-021-01918-y>.
- [19] C. Fang, Z. Yan, X.-J. Zhang, J.-H. Xiao, F. Wang, X.-H. Xu, Stable geometries and magnetic properties in transition-metal-doped Sm<sub>5</sub>Co<sub>19</sub> permanent magnet alloys: insights from DFT, *Sci. China Phys. Mech. Astron.* 68 (4) (2025) 247512, <https://doi.org/10.1007/S11433-024-2593-5>, 2025, 68.
- [20] S. Zhang, S. Ni, Z. Zeng, D. Mo, B. Huang, X. Sun, A sustainable separation strategy for recovering Sm/Co from SmCo magnets with fatty acid and primary amine, *J. Mol. Liq.* 392 (2023) 123490, <https://doi.org/10.1016/J.MOLLIQ.2023.123490>.
- [21] Q. Chen, S. Ni, G. Ai, T. Zhang, X. Sun, A recovery strategy of Sm, Co for waste SmCo magnets by fatty acid based ionic liquids, *Miner. Eng.* 158 (2020), <https://doi.org/10.1016/j.mineng.2020.106581>.
- [22] D.A. Gkika, M. Chalaris, G.Z. Kyzas, Review of methods for obtaining rare Earth elements from recycling and their impact on the environment and human health, *Processing* 12 (2024) 1235, <https://doi.org/10.3390/PR12061235>, 2024, 12, 1235.
- [23] S. Karimi Moghadam, M. Gharavi, A. Asimi Neisiani, D. Crocchio Romano Espinosa, S. Chehreh Chelgani, Hydrometallurgical processes for recycling of SmCo magnets: a comprehensive review, *J. Rare Earths* (2026), <https://doi.org/10.1016/J.JRE.2026.01.005>.
- [24] A. Asimi Neisiani, F. Moosakazemi, S.C. Chelgani, Technical and economic comparison between sodium and ammonium agents in the jarosite precipitation process—an evaluation for industrial applications, *ACS Omega* 8 (2023) 36001–36007, <https://doi.org/10.1021/acsomega.3c03536>.
- [25] Q. Xu, D. Wu, W. Hu, Z. Zhang, X. Liu, F. Yang, Z. Wang, Recycling NdFeB magnets and rare Earth fluorescent materials from electronic waste, *JOM* 76 (3) (2023) 1319–1328, <https://doi.org/10.1007/S11837-023-06235-1>, 2023, 76.
- [26] F. Xiao, W. Hu, J. Zhao, H. Zhu, Technologies of recycling REEs and iron from NdFeB scrap, *Met.* 13 (2023) 779, <https://doi.org/10.3390/MET13040779>, *Page* 779 2023, 13.
- [27] J. Wu, L. Xiao, L. Shen, J.J. Ran, H. Zhong, Y.R. Zhu, H. Chen, Recent advancements in hydrometallurgical recycling technologies of spent lithium-ion battery cathode materials, *Rare Met.* 43 (3) (2023) 879–899, <https://doi.org/10.1007/S12598-023-02437-3>, 2023, 43.
- [28] Management of Electronic Waste, *Manag. Electron. Waste* (2024), <https://doi.org/10.1002/9781119894360>.
- [29] X. Wan, L. Zhou, Z. Chen, L. Shen, M. Chen, Review on pyrometallurgical smelting options for recycling precious and platinum group metals from secondary resources, *Metall. Mater. Trans. B* 2025 (2025) 1–27, <https://doi.org/10.1007/S11663-025-03824-0>.
- [30] Y. Yang, A. Walton, R. Sheridan, K. Güth, R. Gauß, O. Gutfleisch, M. Buchert, B. M. Steenari, T. Van Gerven, P.T. Jones, et al., REE recovery from end-of-life NdFeB permanent magnet scrap: a critical review, *J. Sustain. Metall.* 3 (1) (2016) 122–149, <https://doi.org/10.1007/S40831-016-0090-4>, 2016, 3.
- [31] A. Asimi, K. Gharibi, E. Abkhoshk, F. Moosakazemi, S.C. Chelgani, Effects of operational parameters on the low contaminant jarosite precipitation process—an industrial scale study, *Materials* 13 (2020) 4662, <https://doi.org/10.3390/MA13204662>, 2020, 13, 4662.
- [32] F. Faraji, R. Golmohammadzadeh, C.A. Pickles, Potential and current practices of recycling waste printed circuit boards: a review of the recent progress in pyrometallurgy, *J. Environ. Manag.* 316 (2022) 115242, <https://doi.org/10.1016/J.JENVMAN.2022.115242>.
- [33] M. Kaya, Current WEEE recycling solutions, *Waste Electr. Electron. Equip. Recycl. Aqueous Recover. Methods* (2018) 33–93, <https://doi.org/10.1016/B978-0-08-102057-9.00003-2>.
- [34] S. Rahmati, H. Shalchian, R. Adavodi, I. Birloaga, P. Romano, Evaluation of a hybrid pyro–hydrometallurgical process for the selective leaching of rare Earth elements from spent NdFeB magnets, *Chem. Eng. J.* 521 (2025) 167003, <https://doi.org/10.1016/J.CEJ.2025.167003>.
- [35] M. Orefice, A. Van den Bulck, B. Blanpain, K. Binnemans, Selective roasting of Nd–Fe–B permanent magnets as a pretreatment step for intensified leaching with an ionic liquid, *J. Sustain. Metall.* 6 (1) (2019) 91–102, <https://doi.org/10.1007/S40831-019-00259-1>, 2019, 6.
- [36] A. Khaliq, M.A. Rhamdhani, G. Brooks, S. Masood, Metal extraction processes for electronic waste and existing industrial routes: a review and Australian perspective, *Resour.* 3 (2014) 152–179, <https://doi.org/10.3390/RESOURCES3010152>, 2014, 3, 152–179.
- [37] J.M.D. Coey, Permanent magnet applications, *J. Magn. Magn. Mater.* 248 (2002) 441–456, [https://doi.org/10.1016/S0304-8853\(02\)00335-9](https://doi.org/10.1016/S0304-8853(02)00335-9).
- [38] D. Brown, B.M. Ma, Z. Chen, Developments in the processing and properties of NdFeB-Type permanent magnets, *J. Magn. Magn. Mater.* 248 (2002) 432–440, [https://doi.org/10.1016/S0304-8853\(02\)00334-7](https://doi.org/10.1016/S0304-8853(02)00334-7).
- [39] M. Kaya, An overview of NdFeB magnets recycling technologies, *Curr. Opin. Green Sustainable Chem.* 46 (2024) 100884, <https://doi.org/10.1016/J.COCS.2024.100884>.
- [40] Y. Khan, A.H. Qureshi, On the thermal decomposition of SmCo<sub>5+x</sub>, *Phys. Status Solidi* 28 (1975) 169–174, <https://doi.org/10.1002/pssa.2210280117>.
- [41] M. Orefice, H. Audoor, Z. Li, K. Binnemans, Solvometallurgical route for the recovery of Sm, Co, Cu and Fe from SmCo permanent magnets, *Sep. Purif. Technol.* 219 (2019) 281–289, <https://doi.org/10.1016/J.SEPUR.2019.03.029>.
- [42] X. Li, Z. Li, M. Orefice, K. Binnemans, Metal recovery from spent samarium-cobalt magnets using a trichloride ionic liquid, *ACS Sustain. Chem. Eng.* 7 (2019) 2578–2584, <https://doi.org/10.1021/acssuschemeng.8b05604>.
- [43] N. Swain, S. Mishra, M.R. Acharya, Hydrometallurgical route for recovery and separation of samarium (III) and cobalt (II) from simulated waste solution using Tri-n-Octyl phosphine oxide – a novel pathway for synthesis of samarium and cobalt oxides nanoparticles, *J. Alloys Compd.* 815 (2020), <https://doi.org/10.1016/j.jallcom.2019.152423>.
- [44] Y. Bai, W. Xie, G. Yu, F. Wang, B. Xu, B. Yang, Selective recovery of Sm from Sm-Co magnet scrap by vacuum distillation, *Sep. Purif. Technol.* 348 (2024) 127746, <https://doi.org/10.1016/j.seppur.2024.127746>.
- [45] T. Saito, H. Sato, T. Motegi, K. Kobayashi, Extraction of Sm from sm–fe–n magnets by the glass slag method, *J. Alloys Compd.* 403 (2005) 341–344, <https://doi.org/10.1016/J.JALLCOM.2005.05.029>.
- [46] T. Saito, H. Sato, T. Motegi, Extraction of Sm from Sm–Fe alloys by the glass slag method, *J. Alloys Compd.* 387 (2005) 274–278, <https://doi.org/10.1016/J.JALLCOM.2004.02.064>.
- [47] T. Saito, H. Sato, S. Ozawa, T. Motegi, The extraction of Sm from Sm–Co alloys by the glass slag method, *Mater. Trans.* 44 (2003) 637–640, <https://doi.org/10.2320/MATERTRANS.44.637>.
- [48] E. Emil-Kaya, An integrated hydrometallurgical treatment and combustion process for sustainable production of Sm<sub>2</sub>O<sub>3</sub> nanoparticles from waste SmCo magnets, *Min. Metall. Explor.* 41 (2024) 2047–2056, <https://doi.org/10.1007/s42461-024-01032-z>.
- [49] E. Wiberg, *Lehrbuch Der Anorganischen Chemie*, De Gruyter Brill, 2019, <https://doi.org/10.1515/9783110206845>.
- [50] K. Zhou, A. Wang, D. Zhang, X. Zhang, T. Yang, Sulfuric acid leaching of SmCo alloy waste and separation of samarium from cobalt, *Hydrometallurgy* 174 (2017) 66–70, <https://doi.org/10.1016/J.HYDROMET.2017.09.014>.
- [51] J.Z. Wang, Y.C. Tang, Y.H. Shen, Experimental study on the separation of selected metal elements (sm, Co, Fe, and cu) from nitric acid leachate using specific precipitants, *Recycling* 9 (2024) 1–14, <https://doi.org/10.3390/recycling9060111>.
- [52] K. Sahoo, A.K. Nayak, M.K. Ghosh, K. Sarangi, Preparation of Sm<sub>2</sub>O<sub>3</sub> and Co<sub>3</sub>O<sub>4</sub> from SmCo magnet swarf by hydrometallurgical processing in chloride media, *J. Rare Earths* 36 (2018) 725–732, <https://doi.org/10.1016/J.JRE.2017.12.011>.
- [53] Rare Earth Permanent Magnets, *Rare Earth Perm. Magnets* (1973), <https://doi.org/10.1016/B978-0-12-515450-5.X5001-7>.
- [54] A.K. Nayak, B. Behera, K. Sarangi, M.K. Ghosh, S. Basu, Process flowsheet development for separation of Sm, Co, Cu, and Fe from magnet scrap, *ACS Omega* 6 (2021) 188–196, <https://doi.org/10.1021/acsomega.0c04132>.
- [55] Y. Deng, Y. Zhang, Y. Ding, Recovery of rare earths in different media with novel dicarboxylate based ionic liquid and application to recycle SmCo magnets, *Hydrometallurgy* 210 (2022) 105844, <https://doi.org/10.1016/j.hydromet.2022.105844>.
- [56] X. Liang, Q. Zeng, Recovery of Samarium(III) and Cobalt(II) in synthetic nitric acid solutions using carboxyl functionalized ionic liquids and application to recycling SmCo permanent magnets, *Hydrometallurgy* 216 (2023), <https://doi.org/10.1016/j.hydromet.2022.106016>.